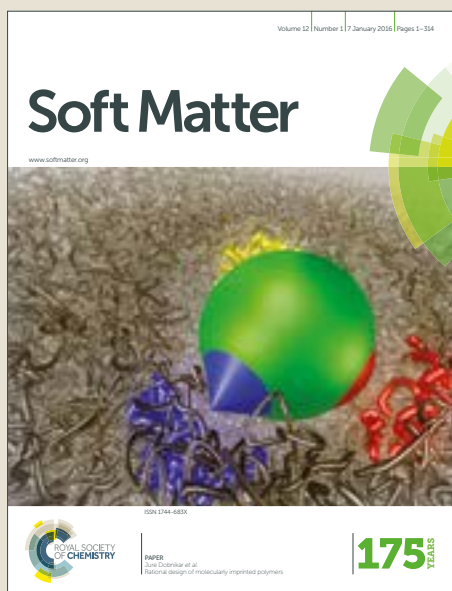


Soft Matter

Accepted Manuscript



This article can be cited before page numbers have been issued, to do this please use: G. Zaldivar, M. B. Samad, M. Conda-Sheridan and M. Tagliacruzchi, *Soft Matter*, 2018, DOI: 10.1039/C8SM00096D.



This is an Accepted Manuscript, which has been through the Royal Society of Chemistry peer review process and has been accepted for publication.

Accepted Manuscripts are published online shortly after acceptance, before technical editing, formatting and proof reading. Using this free service, authors can make their results available to the community, in citable form, before we publish the edited article. We will replace this Accepted Manuscript with the edited and formatted Advance Article as soon as it is available.

You can find more information about Accepted Manuscripts in the [author guidelines](#).

Please note that technical editing may introduce minor changes to the text and/or graphics, which may alter content. The journal's standard [Terms & Conditions](#) and the ethical guidelines, outlined in our [author and reviewer resource centre](#), still apply. In no event shall the Royal Society of Chemistry be held responsible for any errors or omissions in this Accepted Manuscript or any consequences arising from the use of any information it contains.



Journal Name

ARTICLE

Self-assembly of Model Short Triblock Amphiphiles in Dilute Solution

G. Zaldivar^a, M. B. Samad^b, M. Conda-Sheridan^b and M. Tagliazucchi^{a,*}Received 00th January 20xx,
Accepted 00th January 20xx

DOI: 10.1039/x0xx00000x

www.rsc.org/

In this work, a molecular theory is used to study the self-assembly of short diblock and triblock amphiphiles, with head-tail and head-linker-tail structures, respectively. The theory was used to systematically explore the effects of the molecular architecture and the affinity of the solvent for the linker and tail blocks on the relative stability of the different nanostructures formed by the amphiphiles in dilute solution, which include spherical micelles, cylindrical fibers and planar lamellas. Moreover, the theory predicts that each of these nanostructures can adopt two different types of internal organization: i) normal nanostructures with a core composed of tail segments and a corona composed of head segments, and ii) nanostructures with a core formed by linker segments and a corona formed by tail and head segments. The theory predicts the occurrence of a transition from micelle to fiber to lamella when increasing the length of the tail or the linker blocks, which is in qualitative agreement with the geometric packing theory and with experiments in the literature. The theory also predicts a transition from micelle to fiber to lamella as the affinity of the solvent for the tail or linker block is decreased. This result is also in qualitative agreement with experiments in literature but cannot be explained in terms of the geometric packing theory. The molecular theory provides an explanation for this result in terms of the competition between solvophobic attractions among segments in the core and steric repulsions between segments in the corona for the different types of self-assembled nanostructures.

Introduction

The simplest amphiphilic molecules have two well-defined blocks: a solvophilic head and a solvophobic tail. The addition of a third block, with physico-chemical properties different from the tail and head segments (the 'linker' block), expands the possibilities for self-assembly of the molecule.^{1–4} In general, di- and tri-block copolymers have total lengths of hundreds or thousands of monomers (molecular weights in the order of 10–100 kDa). On the other hand, peptide amphiphiles are a subset of short (typically Mw < 1 kDa) di-⁵ and tri-^{6,7} block amphiphiles. These molecules contain one or more alkyl tail(s) covalently attached to a peptide block. The peptide segment can be subdivided into the linker region, with amino acids prone to form strong hydrogen bonds and β -sheet structures (valine, alanine), and a hydrophilic terminal group (glutamic acid, aspartic acid, lysine). Alternatively, the terminal group can be composed by polyamines or poly(ethylene glycol)

groups instead of amino acids.⁸ Peptide amphiphiles can self-assemble in solution, forming micelles, nanofibers, vesicles, nanoribbons and nanosheets.^{6–9} While long ABC triblock copolymers can form complex structures exhibiting patches due to the local aggregation of incompatible blocks,^{10–13} formation of surface patches have not been observed (or reported) in self-assembled structures of peptide amphiphiles, which may be ascribed to the fact that they are shorter than triblock copolymers.

The self-assembling properties of peptide-amphiphiles critically depend on their molecular architecture. For example, Xu et al. have shown that increasing the length of the alkyl tail of peptide amphiphiles in basic media triggered a transition from micelles to fibers.¹⁴ Gore et al. prepared peptide amphiphiles with two alkyl tails per molecule and showed that increasing the tail length leads to a transition from spheroidal micelles to bilayer disk-like aggregates.¹⁵ Stupp and collaborators have studied the effects of the length of the linker and head blocks on the morphology of the system.^{16,17}

In this work, we present a molecular theory for the self-assembly of short neutral diblock and triblock amphiphiles in diluted solution (*i.e.* a solution where the interactions among self-assembled nanostructures are negligible). Inspired by the molecular architecture of peptide amphiphiles, we considered short molecules with strong linker-linker and tail-tail attractive interactions. We studied the self-assembly of these triblock amphiphiles in diluted solution as a function of the

^a INQUIMAE-CONICET and DQIAQF, University of Buenos Aires, School of Sciences, Ciudad Universitaria, Pabellón 2, Ciudad Autónoma de Buenos Aires C1428EHA, Argentina

^b College of Pharmacy, Department of Pharmaceutical Sciences, University of Nebraska Medical Center, Omaha, NE 68198-6125, USA

† Footnotes relating to the title and/or authors should appear here.

Electronic Supplementary Information (ESI) available: [details of any supplementary information available should be included here]. See DOI: 10.1039/x0xx00000x

architecture of the molecule and strength of the interactions. Peptide amphiphiles have been studied using atomistic^{18,19} and coarse-grained^{20–22} molecular dynamics simulations, but these works focused heavily on understanding structural details (at an atomistic scale) of a given type of aggregate rather than predicting the effect of the chemical structure of the amphiphiles (*i.e.* their molecular architecture) on the morphology behavior of the self-assembled structures. Moreover, previous simulation work in the area of peptide amphiphiles^{18–22} and generic short ABC-triblock copolymers^{2,11,23} did not address the thermodynamic stability of the aggregates (with few exceptions²⁴), which is important as it allows to predict the most stable supramolecular structure for a given self-assembling molecule. Therefore, it is not clear whether the sizes and morphologies of the simulated aggregates correspond to the thermodynamically most stable nanostructures. The latter issue is straightforwardly addressed by the theory presented in this work, which allows to calculate the standard chemical potential of the amphiphiles in isolated aggregates of different size and morphology (micelles, fibers, lamellas) fixed on the space. We show that the effect of molecular architecture on the morphology diagram of short triblock amphiphiles can be qualitatively understood in terms of the geometric packing theory, which has very successfully explained the behavior of simple surfactants and diblock copolymers in the past. We also predict the formation of two different types of aggregates, containing cores composed by tail segments (*i.e.* normal structures) or by linker segments. Note that in the latter case, the solvophobic tail block forms part of the solvophilic corona; therefore, aggregates with linkers at the core are only stable for molecules with very short tail blocks. Finally, our calculations predict and explain the micelle→fiber→lamella transition triggered by decreasing the affinity of the solvent for the tail block, which was experimentally observed for diblock copolymers.

Theoretical Methods

Free Energy Functional

Our theoretical approach is based on a molecular theory, developed by Szeleifer and collaborators.^{25–28} This methodology consists in writing down and minimizing the free-energy functional of the system. In the following formulation of the theory, we will assume that micelles and fibers have perfect spherical and cylindrical shapes, respectively, and that they present inhomogeneities only along the radial coordinate. In the same way, we will assume that lamellas are planar and inhomogeneities occur only in the direction normal to the plane. Therefore, the functions in the free energy depend only on one spatial coordinate, r , which is defined as the distance to the center of a spherical micelle, the axis of a cylindrical fiber or the central plane of a lamella. These approximations greatly reduce the computational cost of solving the molecular theory and enable a systematic exploration of the morphology diagram of the system.

The total free energy of an aggregate of N_c amphiphiles is given by:

$$\begin{aligned} \beta F = & \int \rho_c(r) [\ln(\rho_c(r)v_{sol}) - 1] G(r) dr \\ & + \int \rho_{sol}(r) [\ln(\rho_{sol}(r)v_{sol}) - 1] G(r) dr \\ & + \int \rho_c(r) \sum_{\alpha} P(\alpha, r) \ln(P(\alpha, r)) G(r) dr \\ & + \frac{1}{2} \sum_i \sum_j \int \int dr dr' G(r) G(r') \langle n_i(r) \rangle \langle n_j(r') \rangle \beta \varepsilon_{ij} g_{ij}(r, r') \end{aligned} \quad 1$$

where β is $(k_B T)^{-1}$, k_B is Boltzmann's constant and T is the temperature. In all terms of eq. 1, $G(r)dr$ is the volume element at a distance r from the center of the micelle, the axis of the cylindrical fiber or the central plane of the planar lamella. For micelles, $G(r)dr$ is the volume of a spherical shell located at r and with thickness dr , *i.e.* $G(r)dr = 4\pi r^2 dr$. For fibers, $G(r)dr$ is the volume of a cylindrical shell located at r and with thickness dr , $G(r)dr = 2\pi r L dr$ (where L is the length of the fiber). Finally, for the lamella, $G(r)dr$ is the volume of the two layers of thickness dr located at a distance r from the central plane (one above and one below the central plane), $G(r)dr = 2A dr$ (where A is the area of the lamella).

The first two terms in equation 1 account for the free energy associated with the translational entropy of free chains in solution and solvent molecules, respectively. In these terms, $\rho_c(r)$ and $\rho_{sol}(r)$ are the number density of chains and solvent molecules at position r , respectively, and v_{sol} is the molecular volume of the solvent. The third term in eq. 1 accounts for the free energy associated with the conformational entropy of the chains. In this term, $P(\alpha, r)$ is the probability of having an amphiphile in conformation α when its center of mass is at position r . The fourth term in eq. 1 is the free energy associated with the effective segment-segment interactions, in which $\langle n_i(r) \rangle$ is the average number density of segments of type i at position r . In this term, ε_{ij} is the interaction parameter that controls the strength of the attractions between a segment of type i and a segment of type j and $g_{ij}(r, r')$ is a function that accounts for the geometric dependence of the interaction. Note that this term includes only attractive interactions between segments, while steric repulsions are considered exactly for intramolecular segment-segment interactions during the generation of the chain conformations and using a mean-field packing constraint for all other pairs of interactions, as explained below.

The calculation of the density of segments $\langle n_i(r) \rangle$ requires special care. Given a chain at r' in conformation α , let us define $n_i(r; \alpha, r')$ as the number of segments of type i that this chain has in the spherical, cylindrical or planar region between r and $r + dr$. Note that the conformation (α) and position of the center of mass (r') unequivocally define the position of each segment and, therefore, they define the function $n_i(r; \alpha, r')$. To calculate the total number of segments in the spherical, cylindrical or planar region between r and $r + dr$, we multiply $n_i(r; \alpha, r')$ by the probability of having an amphiphile in conformation α when its center of mass is at r' and by the number density of amphiphiles at r' , and then sum over all possible conformations and integrate over all possible positions of the center of mass, r' , including the appropriate Jacobian, $G(r')$:

$$N_i(r) = \sum_{\alpha} \int G(r') n_i(r'; \alpha, r') P(r', \alpha) \rho_c(r') dr'$$

We then divide the number of segments between r and dr , $N_i(r)dr$, by the volume element between r and dr , i.e. $G(r)dr$, in order to finally obtain the density of segments at r :

$$\langle n_i(r) \rangle = \frac{N_i(r)dr}{G(r)dr} = \sum_{\alpha} \int \frac{G(r')}{G(r)} n_i(r'; \alpha, r') P(r', \alpha) \rho_c(r') dr'$$

Note the factor $G(r')/G(r)$ in this equation, which is equal to the ratio of the volume elements where the chain is located and where the density is calculated.

Minimization of the free energy functional

The equilibrium state of the system results from the minimization of the free energy functional with respect to $\rho_c(r)$, $\rho_{sol}(r)$ and $P(\alpha, r)$, subjected to three restrictions: the first constraint is the normalization of the probability distribution function $P(\alpha, r)$ at each position r :

$$\sum_{\alpha} P(\alpha, r) - 1 = 0; \forall r$$

The second restriction is a packing constraint at each position, which results from modeling repulsive intermolecular interactions as hard-core excluded-volume repulsions:

$$\langle \phi_{sol}(r) \rangle + \sum_i \langle \phi_i(r) \rangle - 1 = 0; \forall r$$

where $\langle \phi_i(r) \rangle$ is the volume fraction of a chain segment of type i at r , defined by

$$\langle \phi_i(r) \rangle = \langle n_i(r) \rangle v_i$$

and $\langle \phi_{sol}(r) \rangle$ is the volume fraction of solvent molecules at r , defined as

$$\langle \phi_{sol}(r) \rangle = \rho_{sol}(r) v_{sol}$$

In eq. 6, v_i is the volume of a segment of type i .

The third constraint restricts the integral of the number density of amphiphiles in the system to be equal to their total number, N_c :

$$\int \rho_c(r) G(r) dr = N_c \quad 8$$

The functional to minimize results from including the constraints in eq. 1 through the use of Lagrange multipliers:

$$\mathcal{L} = \beta F + \int \beta \pi(r) G(r) \left(\sum_i \langle \phi_i(r) \rangle - 1 \right) dr \quad 2$$

$$+ \int \beta \lambda(r) G(r) \rho_c(r) \left[\sum_{\alpha} P(\alpha, r) - 1 \right] dr$$

$$+ \kappa \left[N_c - \int \rho_c(r) G(r) dr \right]$$

where $\beta \pi(r)G(r)$ and $\beta \lambda(r)G(r)\rho_c(r)$ are the Lagrange multipliers associated with the packing constraint and the normalization of $P(\alpha, r)$, respectively, and κ is the Lagrange multiplier associated with the restriction on the integral of the number density of chains.

Equations for the number density of the solvent, $\rho_{sol}(r)$, and amphiphiles, $\rho_c(r)$, and for the probability-distribution function of chains conformations, $P(\alpha, r)$, are obtained as outputs from the minimization of the potential \mathcal{L} . The expression resulting from the minimization for the number density of solvent molecules is

$$\rho_{sol}(r) v_{sol} = \exp(-\beta \pi(r) v_{sol})$$

where $\pi(r)$ is physically interpreted as the local osmotic pressure at each position r .

4

The expression for the probability distribution function is

$$P(\alpha, r) = q(r)^{-1} \exp \left(- \int dr' \sum_i n_i(r'; \alpha, r) \beta \pi(r') v_i \right. \\ \left. - \int \int dr' dr'' \sum_i \sum_j n_i(r'; \alpha, r) G(r'') \langle n_j(r'') \rangle \beta \epsilon_{ij} g_{ij}(r', r'') \right)$$

where $q(r)$ is a single-chain internal partition function at position r , which is equal to

$$q(r) = \exp(1 + \beta \lambda(r)) \quad 12$$

6

The expression for the number density of chains resulting from the minimization of the potential \mathcal{L} is

$$\rho_c(r) v_{sol} = q(r) \exp(\kappa) \quad 13$$

7

We are interested in the chemical potential of the amphiphiles within the aggregates. Let us define $F^{\dagger}(N_c)$ as the value of the constrained extremum of the free energy for a system with N_c amphiphiles. In other words, $F^{\dagger}(N_c)$ is the free energy that results from replacing the solution of the optimization obtained for a given value of N_c , eqs. 10-13, into our free energy functional, eq. 1. The chemical potential of the amphiphiles is given by:

$$\beta \mu_c^o = \frac{dF^{\dagger}(N_c)}{dN_c} = \frac{\partial \mathcal{L}[\rho_{sol}, \rho_c, P, \pi, \lambda, \kappa, N_c]}{\partial N_c} = \kappa \quad 14$$

where the first equality follows from the definition of chemical potential and the second equality is a consequence of the envelop theorem.²⁹ This equation reveals the meaning of κ (Lagrange multiplier fixing the total number of amphiphiles in the system) as the standard chemical potential of the amphiphiles within the aggregates. Note that in our calculation, the aggregates are fixed in space and they are in the infinite dilution limit (thus we ignore interactions among aggregates). The superscript in μ_c^o denotes these conditions, following the notation introduced by Israelachvili^{30,31} and then used by other authors.^{25,32,33} While the chemical potential μ_c^o corresponds to amphiphiles within isolated aggregates that lack of their translational degrees of freedom, it incorporates, however, the interactions between amphiphiles inside the aggregates. It is also important to mention that the fibers and lamellas are infinite aggregates, thus in these cases, both F and N_c scale linearly with the length of the fiber (L) or the area of the lamella (A). Therefore, the standard chemical potentials are a function of the number of aggregates per unit length of fiber or the number of aggregates per unit area of lamella, respectively. Combining eqs. 13 and 14 finally results in:

$$\beta\mu_c^o = \ln(\rho_c(r)v_{sol}) - \ln q(r) \quad (\text{for all } r) \quad 15$$

In this equation, the chemical potential contains contributions from the single-chain internal partition function (first term) and the translational entropy of the amphiphiles within the aggregate (second term). The second term arises because we allow the center of mass of the amphiphiles to be located at any position within the aggregate and we explicitly include the translational entropy of the amphiphiles in our free-energy functional. We can integrate equation 15 in the entire system and use the constraint in eq. 8, which results in:

$$\beta\mu_c^o = -\ln Q \quad 16$$

where,

$$Q = \frac{1}{N_c v_{sol}} \int q(r) G(r) dr \quad 17$$

The expression in eq. 16 for the chemical potential demonstrates the consistency of the preset formulation of the theory with previous work.²⁵

Molecular model

We consider linear di- and tri-block amphiphiles. The triblock molecules contain three regions: the solvophobic tail block (formed by n_{tail} tail segments), the linker block (formed by n_{linker} segments), and the solvophilic head block (formed by n_{head} segments). The diblock amphiphiles have only head and tail blocks and thus lack linker segments ($n_{linker} = 0$). The total number of segments forming the chain was fixed to $n_{total} = 15$ in all calculations. We used the same volume for the segments in the three types of blocks, $v_i = 0.113 \text{ nm}^3$, while the solvent molecular volume was set to $v_{sol} = 0.03 \text{ nm}^3$ (approximately the volume of a water molecule). Therefore, in our model, one segment will be roughly equivalent to two or three methylene groups in the tail block or one amino acid in the head and linker blocks of a generic peptide-amphiphile molecule. For simplicity, in this work we only consider linker-linker and tail-tail effective attractive interactions, thus the interactions between all other pairs of segments are set to zero. In other words, we have to set only two interaction parameters, ϵ_{linker} (interactions between linker segments) and ϵ_{tail} (interactions between tail segments). Note that the fact that head segments do not effectively interact with each other means that they are solvophilic. The geometric dependence of the attractive interactions is given by the function $g_{ij}(r, r')$, which is chosen to model the attractive branch of the Lennard-Jones potential (see Supporting Information). The conformations of the chains are sampled with a set of 10^5 conformations (for each position of the center of mass of the amphiphile) which are randomly generated using the Rotational Isomeric State (RIS) model.³⁴ The use of a set of explicit conformations has some advantages over the Gaussian chains typically used in self-consistent field (SCF) theory, for example, explicit conformations have finite maximum extension and they allow to treat exactly intramolecular repulsions by including only self-avoiding conformations in the calculation.³²

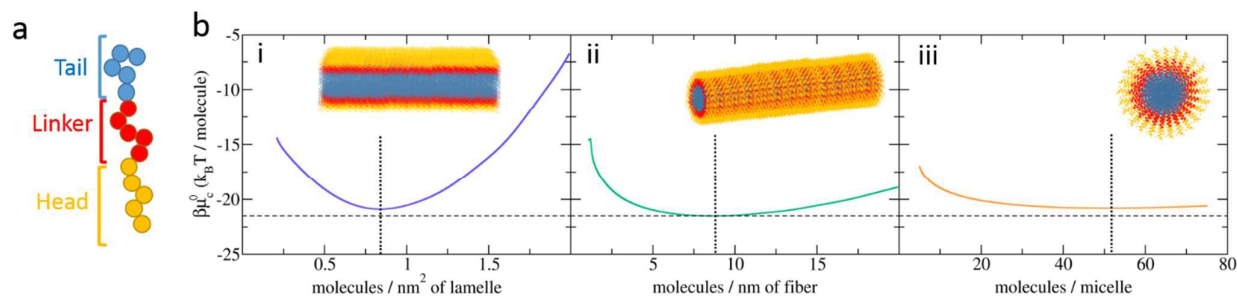


Figure 1. a. Scheme of a triblock amphiphile. b. Chemical potential of an amphiphile molecule, μ_c^o , within different types of supramolecular self-assembled structures: planar lamellas (b-i), cylindrical fibers (b-ii) and spherical micelles (b-iii) as a function of the total number of chains per micelle, the number of chains per unit length of fiber or the number of chains per unit area of lamella. In this calculation, the molecules have five tail segments, five linker segments and five head segments (5:5:5 architecture). For all cases, $\epsilon_{tail} =$

$\epsilon_{\text{linker}} = 3 k_B T/\text{molecule}$. The dotted lines indicate the position of the minima in each plot. The insets in panel b show schemes of the morphologies.

Results

Morphology diagrams of triblock amphiphiles

Figure 1b shows the chemical potential of the amphiphiles, μ_c^o , within self-assembled structures of different morphology (micelle, fiber and lamella) as a function of the total number of molecules (per micelle), the number of molecules per unit length (for fiber) or the number of molecules per unit area (for lamella). Our theory considers infinite fibers and lamellas; therefore we model ideal structures, although in experiments these structures have a finite size. For example, experiments for peptide amphiphiles usually report short fibers^{7,8} (although very long fibers are also rather common³⁵). Ribbons^{7,17} or vesicles (curved bilayers),³⁶ which are usually observed instead of extended planar lamellas.

The calculations in Figure 1 correspond to an amphiphile with a tail:linker:head architecture of 5:5:5 (*i.e.* the tail has five segments, the linker has five segments and the solvophilic head has five segments). All plots of chemical potential vs density or number of molecules in Figure 1b have a minimum (marked with a vertical dotted line),^{25,30} which indicates the presence of stable aggregates. If the chemical potential lacks a minimum, then either μ_c^o monotonically increases with the number or density of molecules, which indicates that the aggregates are unstable with respect to the free amphiphiles in solution, or μ_c^o monotonically decreases with the number or density of molecules, in which case the aggregate will grow indefinitely and form a separated phase.

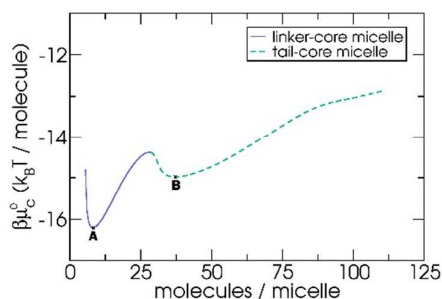


Figure 2. Chemical potential of an amphiphile within a micelle as a function of the aggregation number for a tail:linker:head architecture of 1:8:6. For all cases, $\epsilon_{\text{linker}} = \epsilon_{\text{tail}} = 3 k_B T/\text{molecule}$. The blue line corresponds to cases in which the structure has a core composed of linker segments, and the green line corresponds to cases where the core is composed of tail segments.

The equilibrium morphology and size of the aggregates is the one that corresponds to the global minimum of the chemical potential. In other words, we first find the minimum of the chemical potential, $\mu_c^{o,\text{min}}$, for each type of system (micelle, fiber and lamella) as a function of the number or density of molecules and then select the structure that has the lowest overall $\mu_c^{o,\text{min}}$ as the equilibrium structure. This method of choosing the equilibrium structure is

based on the fact that (given enough time and/or using thermal annealing protocols) molecules will move from structures with high chemical potentials into the structure with the lowest chemical potential (the equilibrium structure). This process requires the chemical potential of the molecules to be independent of the composition of the system (*e.g.* the chemical potential of the amphiphile within the micelles has to be independent of the concentration of the micelles), which is the case of diluted solutions where the interactions between supramolecular aggregates is negligible. Moreover, our analysis neglects the existence of structures with chemical potentials a few $k_B T$ above the global minimum, which coexists with that of lowest chemical potential (in the case of micelles, the distribution of sizes is given by the mass action model, which considers the equilibria between micelles of different sizes^{25,30,37}). In other words, in equilibrium, some degree of dispersion in size and even morphology is always expected.

In some cases, we observed two minima of the chemical potential μ_c^o for a given type of morphology and calculation conditions. For example, in Figure 2, we show μ_c^o vs number of molecules for micelles composed of a amphiphile with a 1:8:6 tail:linker:head architecture. The first minimum (lowest aggregation number) corresponds to micelles with linker segments at the core, while the second minimum is due to micelles with tail segments at the core (*i.e.* “normal” micelles). The structures of these two types of aggregates will be discussed in detail in the last part of the results section.

Effect of molecular architecture on the morphology of the aggregates

Figure 3 shows the morphology diagram of the self-assembled nanostructures with different molecular architectures. The y and x axis of the plot indicate the numbers of linker and tail segments in the molecule, respectively. For each point in the diagram, the number of head segments is fixed by the fact that the total number of segments of the molecule is constant, $n_{\text{total}} = 15$ (dashed lines indicate a constant number of head segments). The labels M, F and L in the diagram correspond to “normal” (core composed by tail segments) micelles, fibers and lamellas, respectively. These structures are the most common in the phase diagram. On the other hand, the structures labelled as M*, F* and L* correspond to micelles, fibers and lamella whose core is composed by linker segments. The M*, F* and L* morphologies mainly occur when the length of the tail block is short and they will be discussed in detail in the last section of the paper. The cases labelled as P and S in the diagram correspond to limiting behaviors. In the limiting case for P, all segments of the molecule are tail or linker segments. These molecules will have strong segment-segment attractions and, therefore, are expected to phase separate. In the limiting case for S, all segments in the molecule are head segments, which are in a good (compatible) solvent and have no effective segment-segment attractions. Therefore, in the S case, the molecules will not form aggregates but will be free in solution. Note that our theory requires aggregates to be both isolated and stable (see Methods and Supporting Information), therefore we are unable to make

predictions for the unlabeled regions in the diagram that are close to the P and S limits.

The diagram in Figure 3 shows that micelles are stable for amphiphiles with long solvophilic head blocks. Increasing the length of the solvophobic tail with fixed linker length stabilizes first the fiber and then the lamella. The same effect is observed when increasing the length of the solvophobic linker while fixing the length of the tail block. Note that the effects of the lengths of the linker and tail blocks on the diagram are similar, although the former appears to slightly stabilize fibers more than the latter.

We can qualitatively compare the results in Figure 3 with experimental results for peptide amphiphiles (a quantitative comparison wouldn't be appropriate considering that peptide amphiphiles are usually charged in solution, while we are modeling neutral amphiphiles). Increasing the length of the alkyl tail (while keeping the lengths of the linker and head blocks constant) have been reported to trigger micelle \rightarrow fiber¹⁴ and micelle \rightarrow lamella¹⁵ transitions, which is in line with our predictions. Increasing the length of hydrophilic head while leaving constant the length of the tail and linker segments, have been shown to lead to a fiber \rightarrow micelle transition; this result is also consistent with the predictions in Figure 3.¹⁶ Finally, Moyer et al.¹⁷ reported a transition from belt-like lamellar assemblies to fibers upon increasing the length of the peptide head block (their molecules did not have well-defined linker and head blocks), which also seems in agreement with our predictions. We can also qualitatively compare our results with the vast literature for diblock copolymers and amphiphiles (note that the labels located on the axes in Figure 3 correspond to cases where the

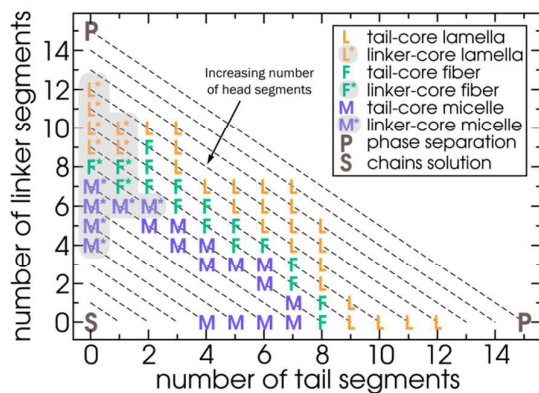


Figure 3. Morphology diagram as a function of the number of tail and linker segments for a total number of segments in the molecule of $n_{\text{total}} = 15$. Calculation parameters: $\epsilon_{\text{linker}} = \epsilon_{\text{tail}} = 3 k_B T$. Dashed lines indicate architectures with a constant number of head segments.

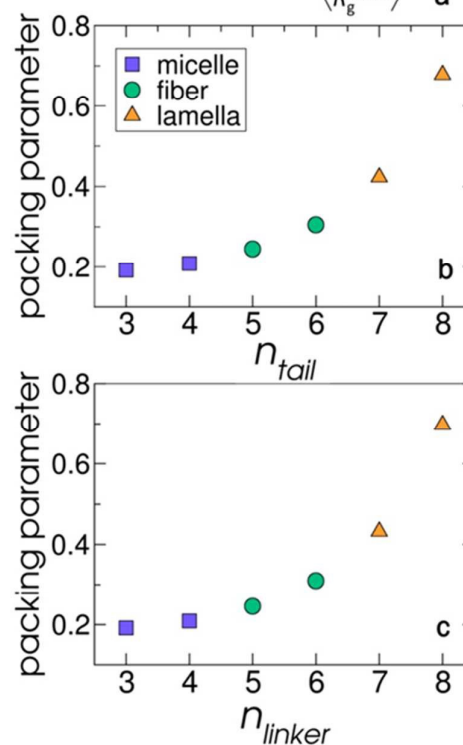
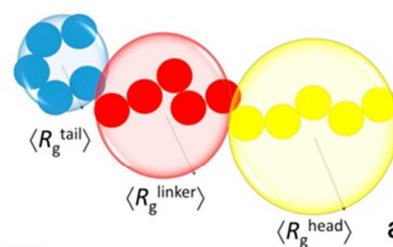


Figure 4. a. Scheme depicting our strategy to estimate the packing parameter for the triblock amphiphiles. The calculated packing parameters (p) are plotted as a function of the number of tail segments (n_{tail} , panel b) and linker segments (n_{linker} , panel c). Calculation parameters: $n_{\text{total}} = 15$ and $\epsilon_{\text{linker}} = \epsilon_{\text{tail}} = 3 k_B T/\text{molecule}$, $n_{\text{linker}} = 4$ (panel b only) and $n_{\text{tail}} = 4$ (panel c only).

number of linker or tail segments is zero, which effectively describes diblock amphiphiles). In the case of diblock amphiphiles, we observe a micelle \rightarrow fiber \rightarrow lamella transition as the length of solvophobic block increases, which qualitatively agrees with experiments for (long) diblock copolymers.^{38,39}

The occurrence of the micelle, fiber and lamella structures in the morphology diagram of Figure 3 is consistent with Israelachvili's geometric packing theory,^{30,31} in which the shape of the molecule dictates the most stable nanostructure. This theory defines the following parameters for the amphiphiles: a_o , which is the head area exposed to the solvent; l_c , which is the characteristic length of the chain; v , which is the molecular volume and p , which is the packing parameter defined by:

$$p = \frac{a_i l_c}{v}$$

The value of p determines the geometry of the structure into which the molecules will pack. Amphiphiles with $p \sim 1$ will have cylindrical shape and thus will pack into a structure with no curvature (lamella). If p is lower than 1, the curvature will be positive and as p decreases, amphiphiles will pack into structures with increasing curvature. Particularly, when $p < 1/3$, chains have conical shape and they will pack into micelles and when $1/3 < p < 1/2$ they have truncated conical shape and will pack into fibers.

In order to estimate the shape of the molecules in our calculation and provide a value for p , we determined the average radius of gyration of each block, $\langle R_g^i \rangle$, where i = tail, linker or head block. The calculation of $\langle R_g^i \rangle$ for the free polymers in solution was done using the same set of calculations employed to solve the molecular theory. As we explain in the Supporting Information, we consider isolated molecules in this calculation and, therefore, we explicitly include the intramolecular attractions by calculating the pairwise interactions instead of modeling these interactions at the mean-field approximation level, as described in the Methods section. We then approximate the molecules by three spherical particles, whose radii are equal to the radii of gyration of each individual block, $\langle R_g^i \rangle$, see scheme in Figure 4a. Thus, we estimate the total volume of the molecule (v) as the sum of the volumes of the three spheres and a_i as the area of the circle defined by the radius of gyration of the head block, $\langle R_g^{head} \rangle$. Following Israelachvili,³⁰ we estimate l_c as the length of the completely stretched molecule. Finally, we obtained p using equation 18 and plotted p as a function of the length of the tail (Figure 4b) or linker (Figure 4c) blocks. We observed that p increases with the lengths of the tail and linker blocks. While the values of p do not exactly predict the morphology of the stable structure, it is still notable that the simple geometric packing theory predicts the general trends observed with the molecular theory. The difference observed between the packing theory and the molecular theory can be attributed to the fact that the packing theory considers that the amphiphiles resemble idealized rigid shapes (e.g. cone, truncated cone, cylinder, etc), while the molecular theory explicitly considers the conformational degrees of freedom of the molecules and their flexibility. Moreover, our methodology to estimate the packing parameter p is somehow arbitrary, therefore, an exact correspondence between the values of p predicted by our method and those proposed in Israelachvili's model is not expected. However, the simple packing theory and our theory agree in the fact that the shape of the molecule is the most important factor dictating the morphology of the aggregates as a function of the molecular architecture.

It is interesting to note that the plots of p vs n_{tail} and n_{linker} (Figures 4b and 4c) are similar, which is in agreement with the similar effects the linker and tail lengths play in determining the morphology of the system represented in Figure 3. Therefore, the main factor governing the morphology of the system is the ratio of the length of the solvophilic head block to the combined lengths of the solvophobic linker and tail blocks.

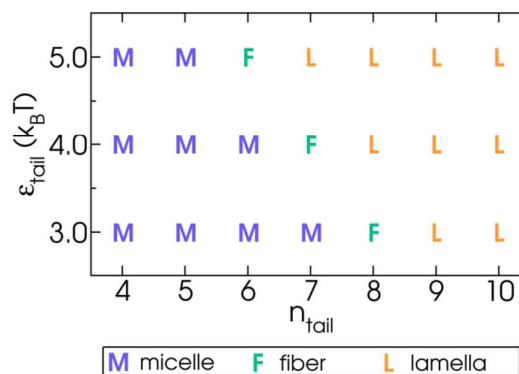


Figure 5. Morphology diagram for a diblock amphiphile as a function of the number of segments in the tail block and the strength of the attractive interactions between them, ϵ_{tail} . Calculation parameters: $n_{linker} = 0$ (diblock amphiphile), $n_{total} = 15$.

Effect of segment-segment attractions on the morphology of the aggregates

For each type of segments, the affinity (or quality) of the solvent controls the strength of the effective segment-segment interactions in our theory (i.e. the effective segment-segment interactions represent the difference between segment-segment and segment-solvent interactions). In other words, the effective interactions between solvophobic segments are strong while the effective interactions between solvophilic segments are weak.

Figure 5 shows the morphology diagram of diblock amphiphiles as a function of the strength of the attractions between tail segments, ϵ_{tail} , and the length of the tail block, n_{tail} . The diagram shows that micelles are stable when the solvophobic tail is short, as we explained in the previous section. For a fixed molecular architecture, increasing the attraction strength between tail segments, ϵ_{tail} , stabilizes structures of decreasing curvature, i.e. increasing ϵ_{tail} leads to a micelle \rightarrow fiber \rightarrow lamella transition. This theoretical prediction can be compared to experimental results for diblock-copolymer micelles in literature. Bang et al.⁴⁰ studied the effect of solvent on the self-assembling of polyisoprene (PI)-polystyrene (PS) block copolymers. As the authors decreased the quality of the solvent for the tail block in the core (PI), the authors observed a micelle \rightarrow fiber \rightarrow vesicle (i.e. curved lamella) transition. In another report, Eisenberg and coworkers^{41,42} studied the morphology of dilute polystyrene(PS)-polyacrylic acid (PAA) diblock copolymers in water:dioxane mixtures. Increasing the fraction of water decreased the quality of the solvent for the PS tail block (note that dioxane is a good solvent for hydrocarbons), which triggered a micelle \rightarrow fiber \rightarrow vesicle transition. Both experimental examples are, therefore, in line with the predictions in Figure 5. It is important to mention that even though the amphiphiles studied in this work are much shorter than the diblock copolymers used in those reports, the general trends predicted by our theoretical model are expected to still be valid for long amphiphiles. Such extrapolation is supported by calculations that show that the morphology diagram of molecules with $n_{total} = 30$ (twice the length used for the calculations in Figure 5, see Figure S5 in the Supporting Information) is qualitatively similar to that for $n_{total} = 15$.

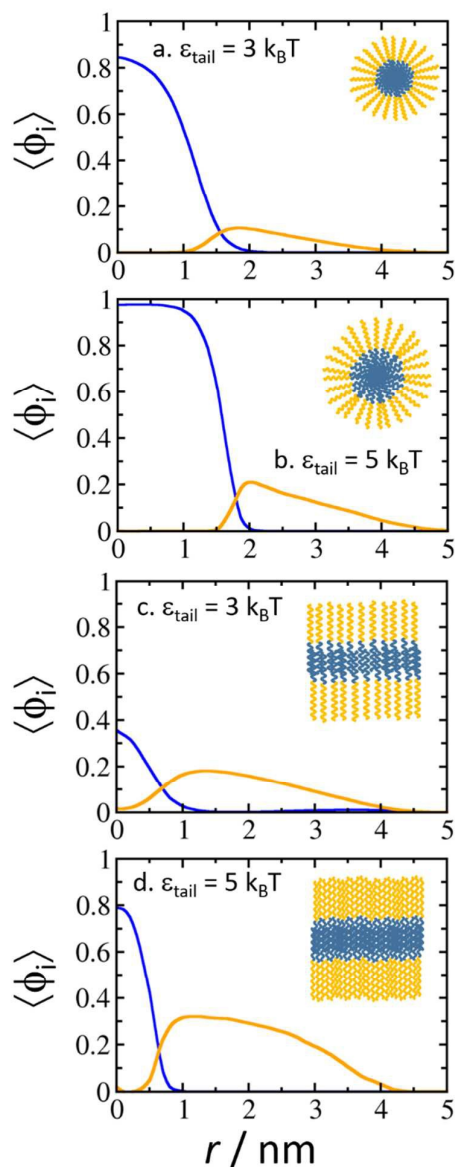


Figure 6. Volume fraction of the tail segments (blue lines) and head segments (yellow lines) as a function of the distance from the center of the aggregates for micelles (a, b) and lamellas (c, d) for $\epsilon_{\text{tail}} = 3 \text{ k}_B T$ (a, c) and $5 \text{ k}_B T$ (b, d). The calculations correspond to a tail:linker:head architecture of 5:0:10 (*i.e.* a diblock molecule).

It is interesting to note that the effect of ϵ_{tail} on the morphology of the aggregates cannot be explained in terms of the geometric packing theory, since increasing ϵ_{tail} for a molecule in solution will decrease the effective size of the tail block and, therefore, led to a lamella \rightarrow fiber \rightarrow micelle transition, which is opposite to our theoretical predictions and the experimental findings in literature. The authors in refs. ^{40–42} explained the solvent-induced transitions by the fact that lowering the affinity of the solvent for the tail block, increases the aggregation number and size of the micelles. Those authors proposed that, at a given critical micellar size, it becomes more favorable to transition to rods and then to vesicles than to continue increasing the size of the micelles. In line with that

assumption, our theory predicts the growth of the aggregation number with ϵ_{tail} : the most stable micelle aggregates have 12, 19 and 29 molecules/micelles for $\epsilon_{\text{tail}} = 3 \text{ k}_B T$, $4 \text{ k}_B T$ and $5 \text{ k}_B T$, respectively. This increase in the aggregation number is accompanied by an increase in the size of the micelle, as we show below. This prediction is also in qualitative agreement with experimental observations for block copolymer micelles that show an increase in size as the quality of the solvent for the core decreases.⁴³

In order to gain insight on the effect of ϵ_{tail} on the morphology of the system, we analyzed the structure of micelles and lamellas for $\epsilon_{\text{tail}} = 3 \text{ k}_B T$ and $5 \text{ k}_B T$ (Figure 6). Note that all these structures correspond to minima in the chemical potential vs density plots (Figure 1). For $\epsilon_{\text{tail}} = 3 \text{ k}_B T$, we observe that the core of the micelle (Figure 6a) has a very large volume fraction of tail segments ($\langle \phi \rangle^{\text{tail}} \sim 0.8 - 0.9$), while the core of the lamella (Figure 6c) has a relatively small volume fraction of tail segments ($\langle \phi \rangle^{\text{tail}} \sim 0.4$) and high solvent content. This result is explained by the fact that the curvature of the micelles allows them to achieve a high density of tail segments at the core without incurring in large segment-segment repulsions in the corona region. On the other hand, the volume fraction of tail segments at the core of the lamella is dictated by the subtle balance of the attractions between tails at the core and repulsions between the head segments at the corona. When increasing ϵ_{tail} from $3 \text{ k}_B T$ to $5 \text{ k}_B T$, the volume fraction of tail segments in the core of the micelle shows almost no change, but the size of the micelle increases (Figure 6b).

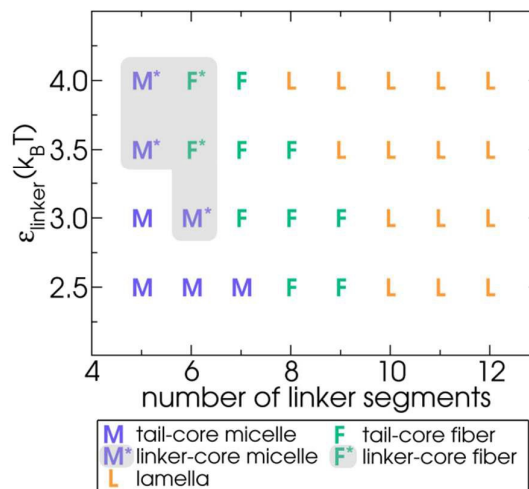


Figure 7. Morphology diagram as a function of the number of linker segments and the strength of the attractions between them for triblock amphiphiles. Calculation parameters: $n_{\text{tail}} = 2$, $n_{\text{total}} = 15$, $\epsilon_{\text{tail}} = 3 \text{ k}_B T$.

On the other hand, the thickness of the lamella remains approximately constant, but the volume fraction of tail segments at the core (Figure 6d) almost doubles. Based on these results, we propose that increasing ϵ_{tail} favors the lamella over the micelle because the lamella can densify its core, increasing the number of favorable contacts between tails segments. On the other hand, the micelle can only increase the number of contacts between tails segments by enlarging the core, but this process cannot be

sustained beyond a certain micelle size (unless head segments are placed in the core, which is energetically unfavorable).

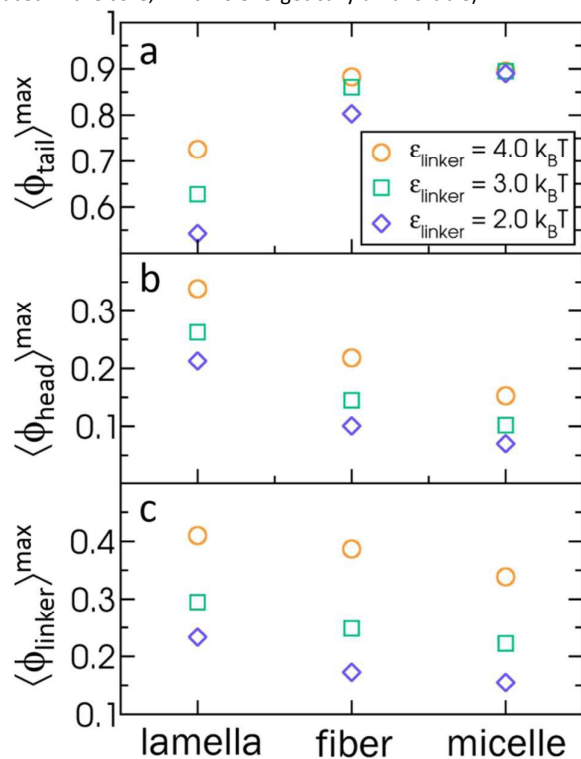


Figure 8. Maximum volume fraction of each type of segment for different structures (all of them having the optimal size or density) as a function of the curvature of the structure for different values of ϵ_{linker} for a 5:4:6 tail:linker:head molecule. For all cases, $\epsilon_{\text{tail}} = 3.0 k_B T$.

In Figure 7, we show the morphology diagram for triblock amphiphiles as a function of the strength of the attractions between linker segments, ϵ_{linker} , and the length of the linker block, n_{linker} . The effect of n_{linker} was already discussed for the morphology diagram in Figure 3 and explained in terms of the geometric packing theory: increasing n_{linker} favors structures with small curvature. Figure 7 shows that increasing ϵ_{linker} results in a micelle \rightarrow fiber \rightarrow lamella transition. This effect is similar to that of increasing interaction parameter between tail segments, ϵ_{tail} (see Figure 5), which can be explained by the fact that increasing ϵ_{linker} has the same effect on the size of the micelles and the density of lamella as increasing ϵ_{tail} . This conclusion is supported by Figure 8, which shows the maximum volume fraction of tail, linker and head segments for the three different morphologies as a function of ϵ_{linker} for a typical triblock architecture. As expected, the increase of the density of tail segments in the core with increasing ϵ_{linker} is much larger for the lamella than for the micelle (Figure 8a).

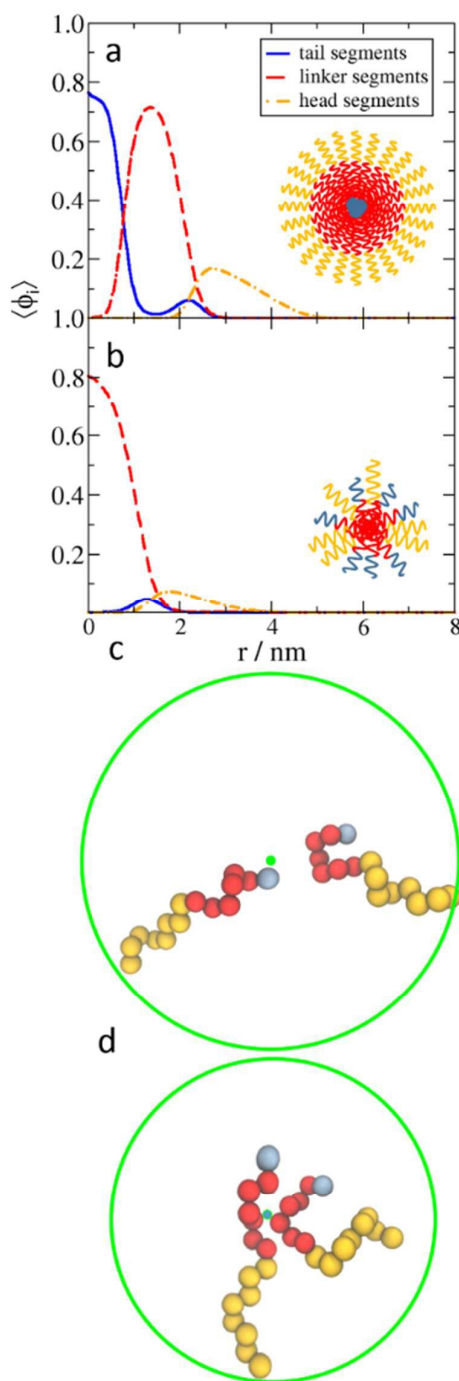


Figure 9. Average volume fractions of each type of segment, $\langle \phi_i(r) \rangle$ as a function of the distance to the center of a micelle (r) for molecules with 1:8:6 tail:linker:head architecture and micelles with tail segments at the core (panel a, M structure) and linker segments at the core (panel b, M* structure). Panels c and d shows two typical conformations for M (panel c) and M* (panel d) micelles. The green dots indicate the centers of the micelles, the green circles are guides for the eye centered on the green dots.

Stability of structures with cores composed of tail segments vs structures with cores composed of linker segments

In the previous sections, we focused our attention on “normal” micelles, fibers and lamella in which the cores were formed by tail segments. We will now turn our attention to the M*, F* and L* morphologies, which contain cores composed of linker segments. We have already shown that these morphologies occur at lower density/aggregation numbers than the M, F and L structures (Figure 2). We also showed that M*, F* and L* structures occur mainly for amphiphiles with short tail blocks (Figure 3). In Figure 9, we plotted the volume fraction of each type of segment for a M micelle (panel a) and a M* micelle (panel b) as a function of the distance to the center of the nanostructure (r). Both plots correspond to the same calculation conditions and molecular architecture (1:8:6 tail:linker:head). Figure 9a shows that the M structure has a core of tail segments, an intermediate section formed by linker segments and a corona exposed to the solvent formed by the head segments. In panels c and d, we show two typical conformations of the amphiphiles for each type of morphology, which we selected from a set of the hundred most probable conformations. The set of most probable conformations for M micelles contain mainly stretched chains, such as the left conformation in Figure 9c. There are a few conformations in which the molecule is bent (see right conformation in Figure 9c). These bent conformations give rise to the secondary maximum, around $r = 2.1$ nm, in the volume fraction profile of tail segments in Figure 9a. Note that this secondary maximum, due to bent conformations, is absent in the plots of Figure 6. We have observed this maximum only for architectures with short tail blocks.

In the M* morphology, the linker segments are collapsed in the core and the outer corona is composed of the tail and head segments (Figure 9b). In this form of supramolecular organization, molecules can be either stretched or bent, since there is no restriction for the angle between tail and head groups as far as the linker is located in the core (see Figure 9d). Based on results of Monte Carlo simulations in literature,² we hypothesize that the corona in the M* can undergo microphase separation. In other words, in order to avoid the incompatibility of the head and tail blocks, the solvophobic tail segments can form aggregates on the surface of the micelle. Since this process would break the spherical symmetry of the system, it cannot be studied with the theory presented in this work as it only considers inhomogeneities in the radial direction.

The relative stability of M*, F* and L* vs M, F and L is governed by the balance of two opposing effects. On one side, placing the linker segments at the core increases the linker local density and, therefore, increases the number of energetically favorable linker-linker contacts, which favors M*, F* and L* morphologies. On the other hand, locating the linker segments at the core requires to place the solvophobic tail segments in the solvophilic corona, which disfavors the M*, F* and L* structures. Therefore, structures with linker segments at the core will be stable only when the free energy penalty of exposing the tail to the solvent and head segments is smaller than the gain of increasing the local density of linker segments in the core. This situation is most likely achieved for molecules with short solvophobic tails.

Conclusions

We have developed a theoretical method to study the self-assembly of di- and triblock neutral amphiphiles. The theory explicitly incorporates the size, shape and conformations of the amphiphiles as well as the steric repulsions and van der Waals attractions among them. We used the theory to systematically study the influence of molecular architecture and quality of the solvent on the stability of the different macromolecular structures formed by the amphiphiles in dilute solution and to construct morphology diagrams for the system. It is important to stress that our theory predicts thermodynamic diagrams of the system, which indicate the equilibrium structures. Note, however, that both triblock copolymers¹⁰ and peptide-amphiphiles⁴⁴ can be trapped in metastable states, *i.e.* local minima of the free energy. Metastable structures cannot be described by the theory reported in this work, but it may be possible to study transitions between them in the future using the recently reported molecular theory/string method formalism.⁴⁵

The theory predicts the occurrence of a micelle→fiber→lamella transition when the size of the tail or linker blocks is increased, which is in qualitative agreement with experimental results for peptide amphiphiles^{14–17} and long diblock copolymers.³⁸ This prediction is also consistent with Israelachvili's packing theory,^{30,31} as we showed by calculating the packing parameter of Israelachvili's theory using our theory. This result suggests that the volume distribution of the molecule is the most important factor dictating the morphology of the aggregates as a function of the molecular architecture. Note, however, that the scope of the geometric packing theory is limited by the fact that it neglects the conformational flexibility of the molecules. On the other hand, our theory explicitly account for the conformational freedom of the amphiphiles, which explains the quantitative differences between the prediction of our model and the simpler geometric packing theory.

Our theory predicts a micelle → fiber → lamella transition when the solvent affinity for the tail or linker blocks is decreased. This effect is in line with experimental results for diblock copolymers,^{40,42} but it cannot be explained by the geometric packing theory. We explain the effect from the fact that micelles can achieve a much higher density of tail segments at the core than lamella because of their high curvature (fibers have a behavior intermediate between micelle and lamella). As the quality of the solvent is lowered, the lamella can increase the favorable tail-tail contacts by increasing the density of the core, but micelles (whose core is already dense in tail segments) can only increase the tail-tail contacts by enlarging the core. This process cannot be sustained beyond a certain micelle size; therefore, as the affinity of the solvent is lowered, the micelles transition first to fibers and then to lamella.

In this work, we addressed model amphiphiles rather than attempting to parametrize our theory for a specific self-assembling molecule. This choice allowed us to qualitatively compare our systematic calculations with different systems in literature and understand the main mechanisms that control the morphology behavior of short di- and triblock amphiphiles. In the future, we plan to modify and parametrize our theory to model specific molecules in order to allow a quantitative comparison with experiments. We are especially interested in the self-assembly behavior of peptide-amphiphiles (PAs), which usually contain charged amino acids; therefore, an important future direction is to extend our theory to model charged species.

Conflicts of interest

There are no conflicts to declare.

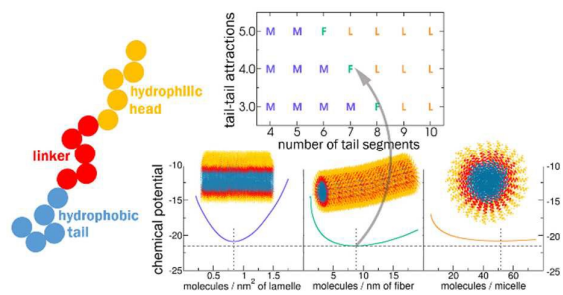
Acknowledgements

MT is a fellow of CONICET. MT acknowledges financial support from Agencia Nacional de Promoción Científica y Tecnológica (ANPCyT) PICT-0099-2015 and PICT 0154-2016. MC-S acknowledges financial support from UNMC (start-up funds). The authors acknowledge a CONICET-NIH Level 1 Bilateral Cooperation Grant.

Notes and references

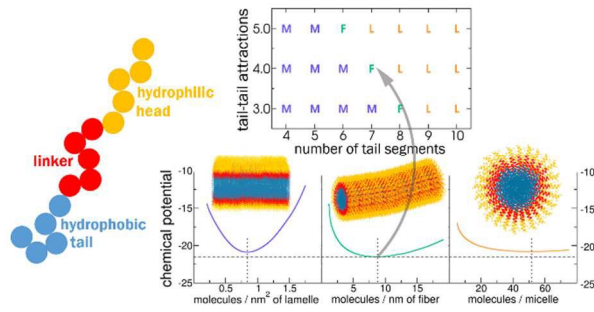
- W. Zheng and Z.-G. Wang, *Macromolecules*, 1995, **28**, 7215–7223.
- Y. Zhu, H. Yu, Y. Wang, J. Cui, W. Kong and W. Jiang, *Soft Matter*, 2012, **8**, 4695–4707.
- G. Yu and A. Eisenberg, *Macromolecules*, 1998, **31**, 5546–5549.
- T. Smart, H. Lomas, M. Massignani, M. V. Flores-Merino, L. R. Perez and G. Battaglia, *Nano Today*, 2008, **3**, 38–46.
- T. Pakalns, K. L. Haverstick, G. B. Fields, J. B. McCarthy, D. L. Mooradian and M. Tirrell, *Biomaterials*, 1999, **20**, 2265–2279.
- H. Cui, M. J. Webber and S. I. Stupp, *Biopolymers*, 2010, **94**, 1–18.
- M. P. Hendricks, K. Sato, L. C. Palmer and S. I. Stupp, *Acc. Chem. Res.*, 2017, **50**, 2440–2448.
- M. B. Samad, Y. S. Chhonker, J. I. Contreras, A. McCarthy, M. M. McClanahan, D. J. Murry and M. Conda-Sheridan, *Macromol. Biosci.*, 2017, **17**, 1700096.
- Y. Chen, H. X. Gan and Y. W. Tong, *Macromolecules*, 2015, **48**, 2647–2653.
- A. H. Gröschel, A. H. E. Müller, J. S. Haataja, O. Borisov, O. Ikkala and T. I. Löbbling, *Nat. Commun.*, 2016, **7**, 12097.
- Y. Zhou, X. Long, X. Xue, W. Qian and C. Zhang, *RSC Adv*, 2015, **5**, 7661–7664.
- C.-A. Fustin, V. Abetz and J.-F. Gohy, *Eur. Phys. J. E Soft Matter Biol. Phys.*, 2005, **16**, 291–302.
- R. Wang, P. Tang, F. Qiu and Y. Yang, *J. Phys. Chem. B*, 2005, **109**, 17120–17127.
- X.-D. Xu, Y. Jin, Y. Liu, X.-Z. Zhang and R.-X. Zhuo, *Colloids Surf. B Biointerfaces*, 2010, **81**, 329–335.
- T. Gore, Y. Dori, Y. Talmon, M. Tirrell and H. Bianco-Peled, *Langmuir*, 2001, **17**, 5352–5360.
- J. E. Goldberger, E. J. Berns, R. Bitton, C. J. Newcomb and S. I. Stupp, *Angew Chem Int Ed Engl*, 2011, **50**, 6292–5.
- T. J. Moyer, H. Cui and S. I. Stupp, *J. Phys. Chem. B*, 2013, **117**, 4604–4610.
- E. D. Tekin, *RSC Adv.*, 2015, **5**, 66582–66590.
- O.-S. Lee, S. I. Stupp and G. C. Schatz, *J. Am. Chem. Soc.*, 2011, **133**, 3677–3683.
- I. W. Fu and H. D. Nguyen, *Biomacromolecules*, 2015, **16**, 2209–2219.
- O.-S. Lee, V. Cho and G. C. Schatz, *Nano Lett.*, 2012, **12**, 4907–4913.
- Y. S. Velichko, S. I. Stupp and M. O. de la Cruz, *J. Phys. Chem. B*, 2008, **112**, 2326–2334.
- T. Jiang, L. Wang, S. Lin, J. Lin and Y. Li, *Langmuir*, 2011, **27**, 6440–6448.
- A. Z. Panagiotopoulos, M. A. Floriano and S. K. Kumar, *Langmuir*, 2002, **18**, 2940–2948.
- C. B. E. Guerin and I. Szleifer, *Langmuir*, 1999, **15**, 7901–7911.
- O. Peleg, M. Tagliazucchi, M. Kroeger, Y. Rabin and I. Szleifer, *ACS Nano*, 2011, **5**, 4737–4747.
- R. Nap, P. Gong and I. Szleifer, *J. Polym. Sci. Part B Polym. Phys.*, 2006, **44**, 2638–2662.
- M. Tagliazucchi, M. Olvera de la Cruz and I. Szleifer, *Proc. Natl. Acad. Sci. USA*, 2010, **107**, 5300–5305.
- M. Carter, *Foundations of mathematical economics*, MIT Press, 2001.
- J. N. Israelachvili, in *Intermolecular and Surface Forces (Third Edition)*, Academic Press, San Diego, 2011, pp. 535–576.
- J. N. Israelachvili, D. J. Mitchell and B. W. Ninham, *J. Chem. Soc. Faraday Trans. 2 Mol. Chem. Phys.*, 1976, **72**, 1525–1568.
- A. D. Mackie, A. Z. Panagiotopoulos and I. Szleifer, *Langmuir*, 1997, **13**, 5022–5031.
- Z. A. Al-Anber, J. Bonet Avalos and A. D. Mackie, *J. Chem. Phys.*, 2005, **122**, 104910.
- P. J. Flory, *J. Chem. Phys.*, 1942, **10**, 51–61.
- M. Conda-Sheridan, S. S. Lee, A. T. Preslar and S. I. Stupp, *Chem. Commun.*, 2014, **50**, 13757–13760.
- S. Santoso, W. Hwang, H. Hartman and S. Zhang, *Nano Lett.*, 2002, **2**, 687–691.
- F. A. García Daza, A. J. Colville and A. D. Mackie, *J. Chem. Phys.*, 2015, **142**, 114902.
- Y. Mai and A. Eisenberg, *Chem. Soc. Rev.*, 2012, **41**, 5969–5985.
- E. B. Zhulina, M. Adam, I. LaRue, S. S. Sheiko and M. Rubinstein, *Macromolecules*, 2005, **38**, 5330–5351.
- J. Bang, S. Jain, Z. Li, T. P. Lodge, J. S. Pedersen, E. Kesselman and Y. Talmon, *Macromolecules*, 2006, **39**, 1199–1208.
- H. Shen and A. Eisenberg, *J. Phys. Chem. B*, 1999, **103**, 9473–9487.
- A. Choucair and A. Eisenberg, *Eur. Phys. J. E Soft Matter*, 2003, **10**, 37–44.
- E. G. Kelley, T. P. Smart, A. J. Jackson, M. O. Sullivan and T. H. Epps, *Soft Matter*, 2011, **7**, 7094–7102.
- F. Tantakitti, J. Boekhoven, X. Wang, R. V. Kazantsev, T. Yu, J. Li, E. Zhuang, R. Zandi, J. H. Ortony, C. J. Newcomb, L. C. Palmer, G. S. Shekhawat, M. O. de la Cruz, G. C. Schatz and S. I. Stupp, *Nat Mater*, 2016, **15**, 469–476.
- I. Gleria, E. Mocskos and M. Tagliazucchi, *Soft Matter*, 2017, **13**, 2362–2370.

Table of Contents



We present a molecular theory to study the morphology diagrams of short diblock and triblock amphiphiles in dilute solution.

Table of Contents



We present a molecular theory to study the morphology diagrams of short diblock and triblock amphiphiles in dilute solution.